Photoinduced Electron Transfer in Squaraine Dyes: Sensitization of Large Band Gap Semiconductors

Martin J. Paterson, Lluís Blancafort,† Sarah Wilsey, and Michael A. Robb*

Department of Chemistry, King's College London, Strand, WC2R 2LS, U.K.

Received: July 1, 2002; In Final Form: August 23, 2002

Squaraine dyes are known to photosensitize large band gap semiconductors via a charge-injection process from a singlet excited state. We have modeled this process with the simplest squaraine chromophore and titanium dioxide (TiO_2). A TiO_2−squaraine excited-state complex has been optimized with an adjacent conical intersection. This suggests that the charge injection from the excited-state squaraine into the conduction band of the semiconductor should be an ultrafast photochemical process in agreement with recent experimental results. In terms of Marcus−Hush electron transfer theory, the charge transfer for the TiO_2−squaraine model occurs in the inverted region, which is a strong indication for the equivalence between electron transfer in the inverted region and radiationless decay through a sloped conical intersection.

Introduction

Squaraine dyes form a class of organic photoconducting materials that have been extensively studied for a variety of technological applications including xerographic photoreceptors,[1] organic solar cells,[2] and optical recording media.[3] They exhibit intense and sharp absorption bands in the visible and are able to photosensitize large band gap semiconductors such as TiO_2 via a charge-injection process,[4−8] where the sensitizer is excited at a longer wavelength than that of the semiconductor band gap, and this is followed by charge transfer from the excited dye to the semiconductor. It is thought that an effective interaction between the excited-state squaraine and the semiconductor surface exists which facilitates the charge-transfer process.

$$\mathrm{Sq} + \mathrm{TiO_2} \xrightarrow{h\nu} {}^1\mathrm{Sq}^* + \mathrm{TiO_2} \rightarrow \mathrm{Sq}^*\cdots\mathrm{TiO_2} \rightarrow \mathrm{Sq}^{\bullet\oplus} + \mathrm{TiO_2}(e^-) \quad (1)$$

In this work the mechanistic features of the photoinduced charge-injection process from a squaraine dye to a large band gap semiconductor has been modeled with the simple TiO_2−squaraine complex shown in Scheme 1.

SCHEME 1

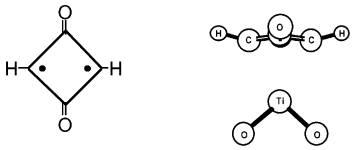

Model Chromophore Model Complex

Experimentally, the dynamics of the charge injection (photogeneration of electron−hole (e−h) pairs) has been studied by femtosecond and picosecond laser spectroscopy.[5,6] In the presence of colloidal TiO_2, squaraine dyes show no appreciable absorption spectral changes. However, the fluorescence emission is strongly quenched, indicative of a competing fast radiationless process. Furthermore, a new absorption band appears around 680 nm after excitation with a 532 nm laser pulse. This new absorption band has been attributed to the formation of the squaraine radical cation. A crown-ether squaraine derivative has been studied using time-resolved transient absorption spectroscopy and the radical cation of this species absorbs at 680 nm.[9] Thus, the rapid quenching and appearance of the radical cation suggests that the excited squaraine undergoes a photochemical reaction in the presence of TiO_2. Studies on the charge-injection dynamics[5] indicate that the new absorption band at 680 nm starts to appear within the duration of the laser pulse which is 18 ps. These observations suggest that charge injection is an ultrafast photochemical process, which is often indicative of the existence of one or more seams of conical intersection on the potential energy surface.[10−13]

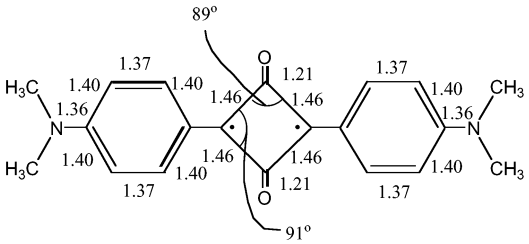

Figure 1. B3LYP/6-31G* S_0 optimized structure of bis(4-(dimethylamino)phenyl) squaraine in D_{2h} symmetry. (Bond lengths in angstroms and bond angles in degrees.)

The electron-transfer rate constants for dyes which can be functionalized with phosphonate or carboxylate groups and "anchored" to the semiconductor surface are significantly higher than for nonfunctionalized dyes.[14,15] The absorption spectra of functionalized dyes recorded in the presence of TiO_2 become broad and red-shifted. This is due to the strong ground-state dye/surface interaction. For non-functionalized dyes, for example, bis(4-(dimethylamino)phenyl) squaraine (Figure 1), where there are no groups that can "anchor" the dye to the semiconductor surface, the ground-state dye/surface interaction is of weak van der Waals type and consequently there are no changes to the absorption spectrum of the squaraine dye. Although the electron-transfer rate constants are lower for nonfunctionalized squaraine dyes, charge injection still occurs

† Institut de Química Computacional, Universitat de Girona, 17071 Spain.

10.1021/jp026418w CCC: $22.00
Published on Web 11/06/2002

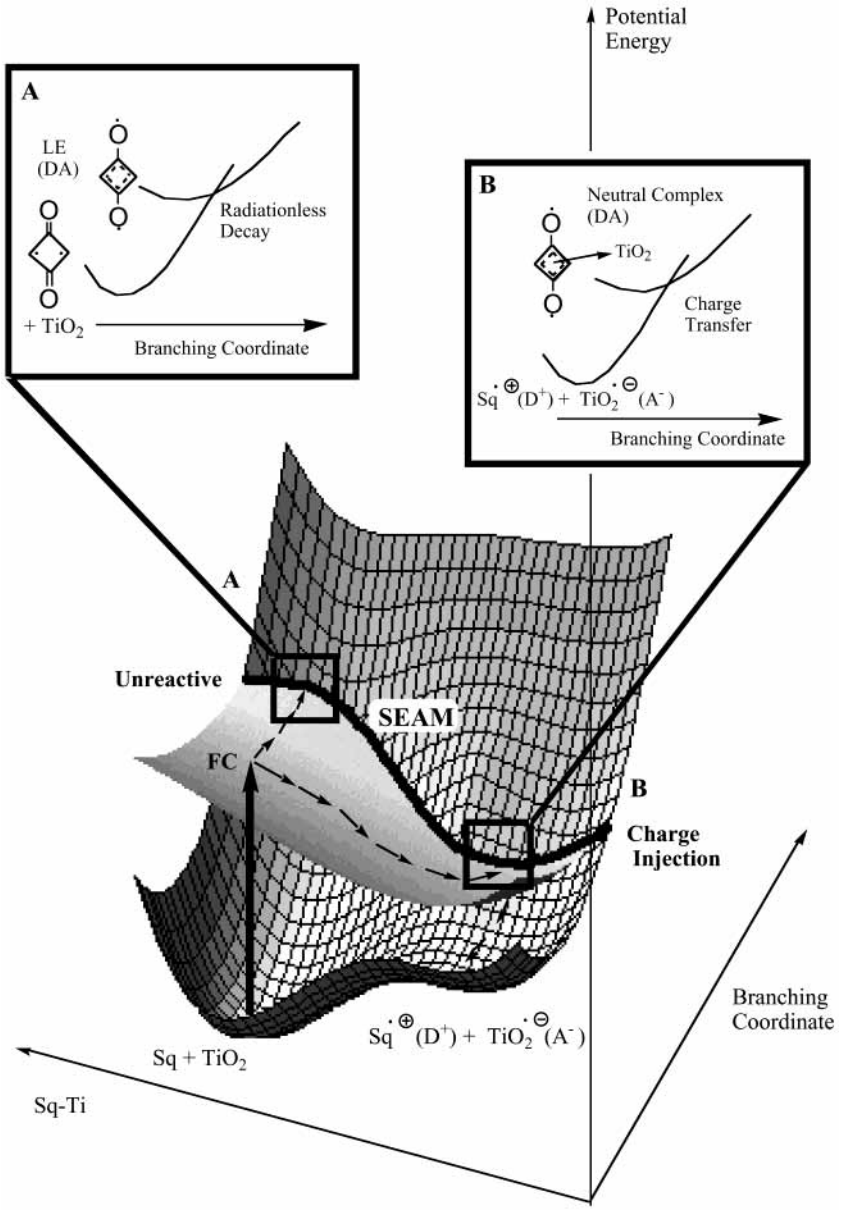

Figure 2. Adiabatic potential energy surface topology. The squaraine is locally excited which leads to interaction with TiO_2 and ultimately to the charge-transfer species via a sloped conical intersection.

with an appreciable rate constant.[5,6] It is thought that the excited state of the dye interacts strongly with the semiconductor and that it is this interaction which is responsible for the intermolecular charge-transfer characteristics of squaraine dyes.

The role of conical intersections in the photochemical reactions of organic molecules has been demonstrated in theoretical ab initio studies.[10−13] The conical intersection can act as an efficient decay funnel from the excited state to the ground-state surface leading to barrierless, ultrafast photochemical processes or thermally activated processes with longer lifetimes. Computations have shown that decay through an intersection can be associated with a photochemical reaction or an unreactive, photophysical path. Conical intersections span n-2-dimensional hyperlines (where n is the number of vibrational degrees of freedom) where the degeneracy persists, called the intersection space.[16] There are two directions that lift the degeneracy, and these define the branching space.[16] One can optimize the geometry of the lowest energy point on the conical intersection.[17] However, the crossing from the excited to the ground state can take place over a whole region of the seam of intersection. In addition, the reaction path may not lie in the branching space itself.

In the discussion of our results on a model TiO_2−squaraine complex we will show that the salient features of the charge-injection process can be understood by considering two points (A and B in Figure 2) on the conical intersection hyperline at different squaraine−TiO_2 distances. The overall reactivity picture is given in Figure 2, where the relevant critical points and calculated reaction paths are grouped schematically. The *two-dimensional branching space* (indicated as a one-dimensional branching coordinate in Figure 2) corresponds to geometrical changes in the squaraine dye itself (involving the recoupling of the π-system on the squaraine) while *the reaction path* is the squaraine−TiO_2 distance (Sq−Ti in Figure 2).

As suggested in Figure 2, the charge-injection process (indicated by the reaction path from the Franck−Condon (FC) region to region B), follows three steps: (1) excitation of the squaraine dye, (2) formation of an excited-state complex (near region B) between the excited dye and the neutral TiO_2 molecule, and (3) transfer of an electron from the squaraine to

the titanium dioxide molecule via a conical intersection (in region B) between the excited state of the neutral species and the ground-state ion pair. Figure 2 also shows an alternative pathway where the excitation energy of the squaraine is dissipated without reaction at another point on the conical intersection seam (region A). The competition between decay at A or B controls the efficiency of the charge injection. Thus the charge-injection process is dominated by two types of nuclear coordinate, the *reaction path* involving the intermolecular separation (Sq−Ti), and the *radiationless decay coordinates* (the branching space) dominated by the squaraine intramolecular motions. The radiationless decay can take place at any point along the seam of intersection. If the squaraine chromophore is held close to a titanium surface site then a complex can form and the charge-injection process takes place. Otherwise, radiationless deactivation will occur through region A.

We would argue that our simple model system (Scheme 1) in the gas phase, can yield mechanistic results that are relevant for the condensed phase problem. The conical intersection we have characterized describes a degeneracy between the neutral state and a charge-transfer state (involving a radical anion state of TiO_2) of our model complex. A recent nonadiabatic molecular dynamics simulation of light-induced electron transfer from an organic dye to a TiO_2 semiconductor surface made out of TiO_2 molecules[18] shows that about 20% of the acceptor state density after the charge transfer is located on a single Ti atom of the first surface layer. This justifies the use of our model, because the charge is significantly localized on one molecule. In the solid state, there will be a continuum of charge-transfer states, and this will enhance the efficiency of the charge injection with respect to our orbital-based model. Furthermore, as our mechanism for the charge-transfer step involves mainly a nuclear coordinate of the squaraine dye itself, the details of the structure of the titanium dioxide lattice are not important. On the other hand, only a dynamics study can directly evaluate the role of vibrationally hot states of the excited chromophore, but our results suggest that a carbonyl bond stretching mode that is excited in the Franck−Condon region is also important for the charge injection, thus increasing the efficiency of the process.

Finally, our mechanism depicted in Figure 2 demonstrates a concept, which is of more general interest. The third step of the mechanism outlined above, eq 1, corresponds to electron transfer in an inverted Marcus region and involves radiationless decay in photoinduced electron transfer.[19] Our previous calculations for ground-state electron transfer have demonstrated that in the full space of nuclear degrees of freedom, the Marcus crossing region is centered on a conical intersection.[20] As we discuss below in detail, calculations carried out in this paper strongly suggest that the inverted Marcus region is equivalent to a sloped conical intersection, where the minima of the crossing states lie on the same side of the intersection.

Computational Details

Calculations on the model squaraine chromophore (Scheme 1) were performed using CASSCF with a 6-31G* basis set. The active space chosen was a six orbital, six electron space which includes all π electrons and molecular orbitals formed from p_π atomic orbitals. In this way it was possible to represent the ground state and the lowest $\pi \rightarrow \pi^*$ excited states.

Bis(4-(dimethylamino)phenyl) squaraine (Figure 1) was studied in order to calibrate the results obtained with the smaller model squaraine shown in Scheme 1. The geometry of bis(4-(dimethylamino)phenyl) squaraine was optimized with density functional theory (B3LYP[21]) using a 6-31G* basis set. Excitation energies were then calculated using time-dependent density functional theory[22] with the same basis set.

The analysis of the MC−SCF wave functions were carried out using the spin-exchange density[23] using localized active orbitals obtained with the Boys method.[24] The spin-exchange density is a two-particle density matrix which can be obtained from a configuration interaction problem as the expectation value of the following operator,

$$P_{ij} = \left\langle \frac{1}{2}(\hat{E}_{ij}^{\alpha\alpha}\hat{E}_{ji}^{\beta\beta} + \hat{E}_{ij}^{\beta\beta}\hat{E}_{ji}^{\alpha\alpha} + [\hat{E}_{ij}^{\alpha\alpha}\hat{E}_{ji}^{\alpha\alpha} - \hat{E}_{ii}^{\alpha\alpha}] + [\hat{E}_{ij}^{\beta\beta}\hat{E}_{ji}^{\beta\beta} - \hat{E}_{ii}^{\beta\beta}]) \right\rangle \quad (2)$$

where the $\hat{E}_{ij}^{\sigma\sigma} = a_{i\sigma}^{+} a_{j\sigma}$ are the standard generators of the unitary group U(n) with $\sigma = \alpha$ or β.

The P_{ij} matrix elements have a simple interpretation which helps one to understand the spin coupling. For a single configuration perfectly paired valence bond (VB) wave function the P_{ij} have values of $+1$ for a singlet coupled pair, -1 for a triplet coupled pair, and $-1/2$ when the pair is uncoupled. Configuration interaction will cause the actual values computed to differ from these idealized values and it is common to take a positive P_{ij} as singlet coupled and a negative P_{ij} as uncoupled. The P_{ij} values allow us to differentiate the π-bonding schemes in the ground and first $\pi\pi^*$ excited state of the model squaraine chromophore.

The CASSCF calculations of the charge-transfer process to TiO_2 (region B in Figure 2) were performed using a CAS(6,7) active space which includes the CAS(6,6) active space of the model squaraine (Scheme 1) plus a TiO_2 "$3d_{yz}$" orbital directed toward the squaraine. This active space was used to optimize both the squaraine−TiO_2 complex and the conical intersection between S_0 and S_1. The geometries were optimized using state-averaged orbitals (weights of 0.5 for each state) with a 6-31G* basis.

At the conical intersection in region B in Figure 2 we need to demonstrate the existence of at least one ground-state reaction path starting from this conical intersection. For a photochemical reaction we have extended the intrinsic reaction coordinate (IRC) method to deal with the case of reaction paths from the conical intersection.[25] This involves the computation of an initial relaxation direction (IRD), which is a minimum on an $(n-1)$-dimensional hyperspherical cross-section of the potential energy hypersurface, where the search is carried out in a subspace orthogonal to a vector centered at the conical intersection. In our studies, the search vectors used were the gradient difference and derivative coupling vectors.

All calculations were performed on an IBM RS/6000 SP2 using a development version of the GAUSSIAN[26] quantum chemical program.

Results

The Excited States of Bis(4-(dimethylamino)phenyl) Squaraine. Bis(4-(dimethylamino)phenyl) squaraine (Figure 1) was studied in order to calibrate the results obtained with the small model squaraine chromophore (Scheme 1). The ground-state geometry was optimized using B3LYP with a 6-31G* basis. The optimizations were carried out in D_{2h}, C_{2v}, and C_s symmetry and with no symmetry constraints. The different molecular symmetries arise from the possible twisting of the methyl groups on the nitrogen atoms. The D_{2h} geometry was found to be the most stable, however the potential energy surface

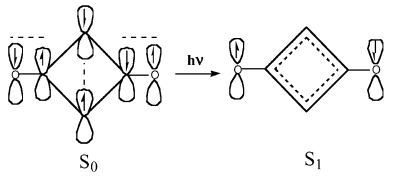

Figure 3. Schematic representation of the $S_0 \rightarrow S_1(p\pi^*)$ electronic transition. CO bonds become uncoupled and a four electron ring system is formed.

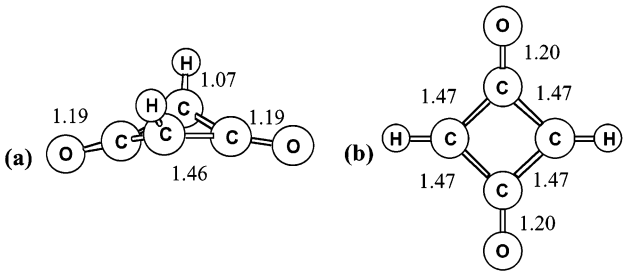

Figure 4. (a) CAS(6,6) optimized S_0 geometry. True minimum with C_{2v} symmetry. Central pyramidalised carbons highlight biradicaloid nature of species. (b) D_{2h} minimum (transition state in C_{2v} space of coordinates) which better represents the squaraine chromophore in the molecular environment. (Bond lengths in angstroms.)

TABLE 1: Energetics of Isolated Squaraine Chromophore

	energy (au)	ΔE (relative to S_0 minimum, kcal mol^{-1})
S_0 minimum (C_{2v}) (Figure 4a)	−302.3287	0.0
S_1 FC (C_{2v})	−302.0900	149.8
S_0 TS (D_{2h}) (Figure 4b)	−302.2891	24.8
S_1 FC (D_{2h})	−302.1978	82.1
S_1 TS (D_{2h}) (Figure 6)	−302.2252	64.9
$S_{0/1}$ CI (D_{2h}) (Figure 6)	−302.2000	80.6
S_1 minimum(C_{2v}) (Figure 7)	−302.2400	55.7
$S_{0/1}$ CI (C_{2v}) (Figure 7)	−302.2385	56.6

is very flat along the torsional coordinate. The optimized geometrical parameters in D_{2h} symmetry are shown in Figure 1.

Time-dependent density functional theory (TDDFT) calculations were carried out at the D_{2h} minimum geometry. The two lowest energy transitions were computed to be at 634 nm ($^1B_{3g}$) and 524 nm ($^1B_{3u}$). The 634 nm transition has a calculated oscillator strength of almost zero and corresponds to a $n\rightarrow\pi^*$ state. The 524 nm transition has an oscillator strength of 1.32 and corresponds to the HOMO → LUMO, $\pi\rightarrow\pi^*$ excitation, which is an allowed transition. In both the $n\rightarrow\pi^*$ and $\pi\rightarrow\pi^*$ visible transitions, the same primary electronic effect involves transfer of electron density from the oxygen atoms into the cyclobutane ring and a schematic valence bond (VB) picture is given in Figure 3. Our computed TDDFT excitation energies compare favorably with the experimental values of 630 and 532 nm obtained for a similar dye.[9]

Most of the experimental work done on the intermolecular charge-transfer characteristics of squaraine dyes involves pumping of the first $\pi\pi^*$ state.[5−9,27−29] The TDDFT computations suggest that the lowest energy singlet transitions involve a redistribution of the electrons localized on the central ring unit. Thus the simple model squaraine chromophore (Scheme 1) should reproduce the qualitative features of the photophysics of a squaraine dye associated with excitation in the visible region.

Photophysics of the Isolated Model Squaraine Chromophore. The CASSCF optimized biradical ground-state geometries of the model squaraine chromophore are given in Figure 4, with the corresponding energies in Table 1. There

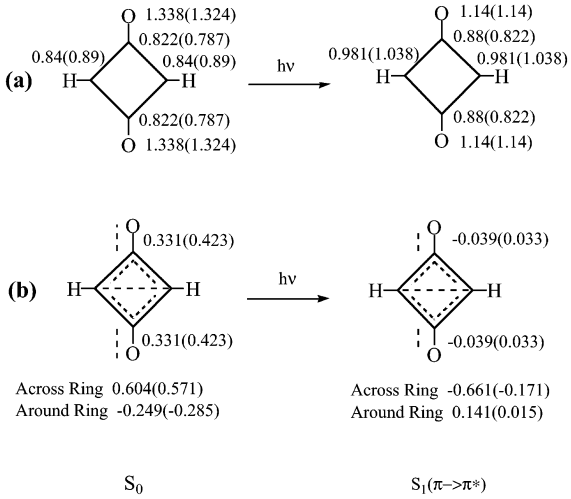

Figure 5. One electron density matrix for (a) S_0 and (b) $S_1(\pi\pi^*)$. Spin-exchange density matrix elements (P_{ij}) for (c) S_0 and (d) $S_1(\pi\pi^*)$ calculated at S_0 D_{2h} transition state geometry. Values in parentheses are those calculated at the C_{2v} minimum geometry.

are two equivalent S_0 minima with C_{2v} symmetry (Figure 4a) and a transition structure with D_{2h} symmetry (Figure 4b) with an associated inversion barrier of 24.8 kcal mol^{-1}. The D_{2h} transition structure is a better representation of the squaraine moiety in a dye such as bis(4-(dimethylamino)phenyl) squaraine where bulky phenyl groups force planarity in the ground state. The geometry of the squaraine chromophore in bis(4-(dimethylamino)phenyl) squaraine (Figure 1) is essentially identical to that of the optimized geometry of the model squaraine chromophore in D_{2h} symmetry (Figure 4b). The CASSCF $\pi\rightarrow\pi^*$ vertical excitation energy for the D_{2h} structure is 520 nm in good agreement with the TDDFT value (524 nm) computed for the real system. The experimental values of the $\pi\pi^*$ vertical excitation energies of squaraine dyes are normally in the range (500−550 nm).[5−9,27−29]

The nature of the electronic structure of the ground state is depicted in Figure 3. The VB structure (Scheme 1) suggests that this species is biradicaloid in nature and one can observe the associated pyramidalisation of the C_{2v} C−H carbons in Figure 4. The spin-exchange density matrix element (P_{ij}) (Figure 5c) for the coupling of electrons across the cyclobutane ring is large and positive (+0.57), consistent with a singlet biradical in the ground state. Both CO bonds are formally coupled as double bonds as indicated by P_{ij} values of +0.423 between the p_π atomic orbitals of the carbon and oxygen.

The nature of the charge reorganization in the $\pi\rightarrow\pi^*$ vertical excitation is shown schematically in Figure 3 and can be seen from the change in the π-electron densities (Figure 5a,b) on excitation. Electron density is transferred from the oxygen atoms into the ring in agreement with semiempirical calculations previously carried out on bis(4-(dimethylamino)phenyl) squaraine.[30] Comparing Figure 5a,b, one can see that the electron density on the oxygen atoms is reduced from 1.3 electrons in the ground state to 1.14 electrons in the S_1 state. Further, the electron density on all of the ring carbons increases upon excitation, especially on the C−H carbons where the density goes from 0.84 electrons in S_0 to 0.981 electrons in S_1.

The change in the spin coupling upon excitation is also evident from the change in the P_{ij} values (Figure 5c,d). The CO bonds have P_{ij} values of +0.331 in the ground state which change to negative values of −0.039 in S_1, indicating that the CO π-bonding electrons have become uncoupled upon excitation. In contrast, the P_{ij} values suggest that the electrons around

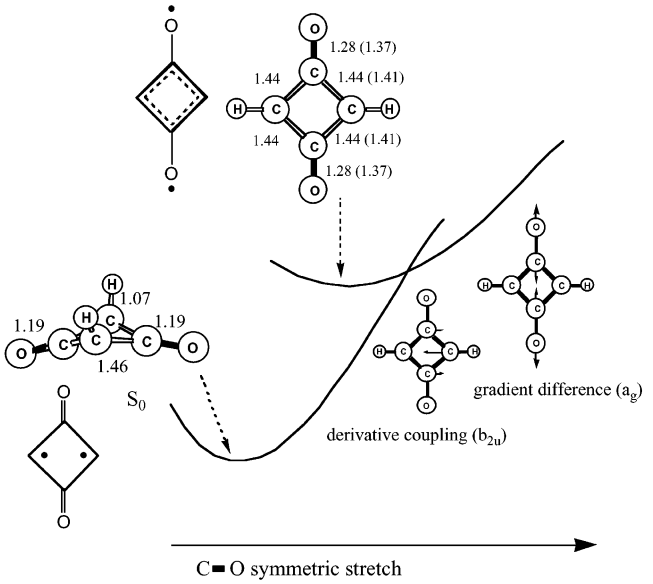

Figure 6. Sloped conical intersection between S_0 and $S_1(\pi\pi^*)$. This point on the intersection seam has D_{2h} symmetry and is a saddle point in the degenerate subspace. (Bond lengths in angstroms)

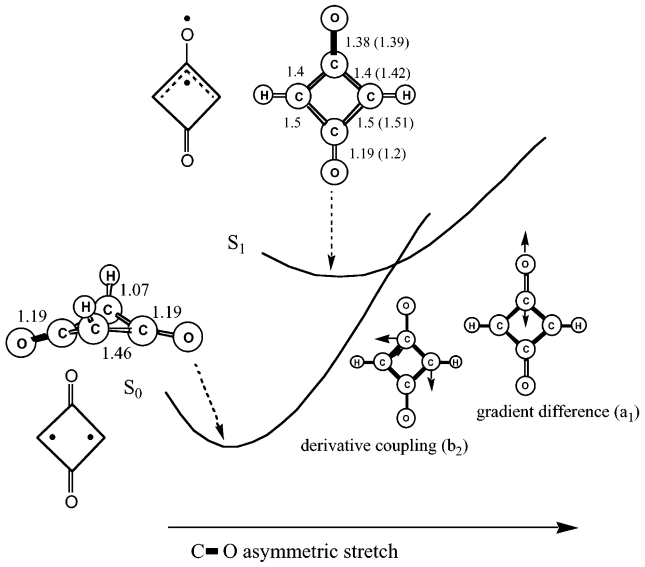

Figure 7. Sloped conical intersection between S_0 and $S_1(\pi\pi^*)$. This point on the intersection seam has C_{2v} symmetry and is a minimum in the degenerate subspace. (Bond lengths in angstroms.)

the ring go from uncoupled (−0.249) in S_0 to coupled (+0.141) in S_1, while the electrons across the ring (P_{ij} between the two C−H carbons) become completely uncoupled. Thus the excitation causes the CO bonds to become uncoupled and there is a transfer of electron density from the CO double bonds into the four-membered cyclobutane ring (Figure 5) creating a four electron ring system as shown in Figure 3.

We now turn to a discussion of the topology of the $\pi\rightarrow\pi^*$ S_1 surface. The change in spin coupling leads to relaxation of both the CO bonds and the ring structure following excitation. There are two low-energy domains of the S_1 surface, one associated with symmetric CO stretching from the FC point (retaining D_{2h} symmetry), and a second region, associated with asymmetric motion of the CO bonds and ring structure. Each of the two domains contains a "local" minimum (optimized with state-averaged orbitals) with a surface crossing at a higher energy (i.e. a point on a conical intersection seam with sloped topology, see Figures 6 and 7). The D_{2h} minimum structure in Figure 6 is in fact a transition structure in the full space of coordinates and connects two equivalent forms of the C_{2v} minimum shown in Figure 7. Note the C_2 axis is along the CO bonds, while in the ground-state C_{2v} minimum, the C_2 axis passes through the center of the ring orthogonal to the molecular plane. The transition vector is indicated in Figure 8.

The sloped conical intersection with C_{2v} symmetry (Figure 7) lies just above the true minima. The origin of this degeneracy can be understood in terms of a simple valence bond argument. If one of the CO bonds is stretched then the energy of the S_0 state will rise steeply since in the ground state the CO π electrons are fully coupled. The S_1 state, on the other hand, has only one fully coupled CO π bond while the other is uncoupled, and is therefore stabilized by the stretching of one CO bond. The two states are therefore degenerate at geometries close to the S_1 minima. There is an equivalent C_{2v} conical intersection which involves the uncoupling of the other CO bond. The conical intersection with D_{2h} symmetry (Figure 6) is connected to both of these degenerate regions and is thus a saddle point in the $(n-2)$-dimensional degenerate subspace.

Finally, we note the recent theoretical and experimental studies of Gude and Rettig[31] on indolinylidenemethyl squaraine and piperidino squaraine. They note that both the n$\rightarrow\pi^*$ and

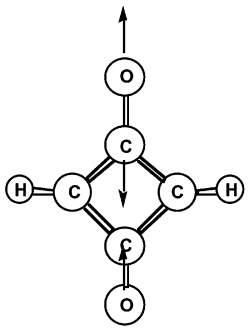

Figure 8. Transition vector associated with S_1 D_{2h} transition state.

$\pi\rightarrow\pi^*$ excitations correspond to an electron flow from the carbonyl unit to the central part of the molecule in agreement with our results. Their computed excitation energies are higher than our calculated values although the model chromophores which they use are somewhat different from ours. They also discuss a possible twisting mode, which when coupled to the relaxation of the central unit, could give rise to a conical intersection and possibly radiationless decay. However, the proposed decay path involving twisting seems to play only a minor role for our reference compound bis(4-dimethylaminophenyl) squaraine, as shown by its relatively high experimental fluorescence quantum yield. Thus, the model calculations do not need to consider the bond-twisting mechanism. At the same time, the experimental data suggest that the bond recoupling deactivation path calculated for unsubstituted squaraines will operate on the reference compound with low efficiency (i.e., higher barriers). Thus, our simple squaraine model reproduces the photophysics of the reference bis(4-dimethylaminophenyl) squaraine qualitatively. Differing substituent groups on squaraine dyes of this type will affect this energy difference but not the general mechanism for radiationless deactivation.

Modeling the Intermolecular Charge-Transfer Process. TiO_2 is a wide band gap semiconductor with a band gap of 3.1 eV.[32] The upper valence band is composed of oxygen "2p" orbitals and the conduction band is composed of titanium "3d" orbitals. The conduction band is split into two distinct bands that can be thought of as arising from the crystal field splitting of the titanium "3d" orbitals in an octahedral ligand field.[32] In

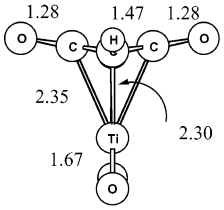

Figure 9. $S_1(Sq^*/TiO_2)$ minimum geometry (excited-state complex minimum energy structure). Optimized with CAS(6,7)/6-31G*(6D) with state-averaged orbitals. (Bond lengths in angstroms.)

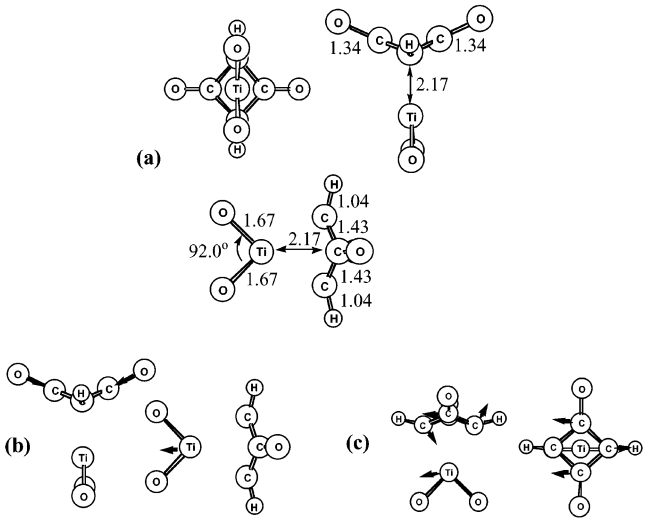

Figure 10. (a) Optimized conical intersection (CAS(6,7)/6-31G*(6D)) between Sq^*/TiO_2 and $Sq^{\cdot+}/TiO_2^{\cdot-}$. (b) Gradient difference vector (a_1). (c) Derivative coupling vector (b_2). (Bond lengths in angstroms.)

the crystal, each titanium atom is coordinated to six oxygen atoms and has a site symmetry of D_{2h}, but it is very close to O_h symmetry. In the $[TiO_6]^{8-}$ ion, the lowest energy virtual orbitals are the t_{2g} and e_g "3d" orbital sets. It is these two orbital sets which give rise to the first two conduction bands in bulk TiO_2.

In an isolated TiO_2 molecule the HOMO is oxygen "2p" and the LUMO is titanium "3d". It has previously been noted that the electronic structure of different small $(TiO_2)_n$ clusters is very similar.[33] The relatively simple electronic structure of TiO_2 allows a straightforward correlation between the HOMO−LUMO levels of TiO_2 to $(TiO_2)_n$, then to the band structure of TiO_2 in the bulk. We have thus used a single TiO_2 molecule interacting with the model squaraine chromophore in order to study the charge-injection process. A "3d" orbital resembling the LUMO of isolated TiO_2 was added to the active space used to study the squaraine chromophore.

A stable excited-state squaraine−TiO_2 complex (region B in Figure 2) arises when the four-electron ring of the excited squaraine acts as a donor ligand to the titanium center. An S_1 minimum (Figure 9) of this complex was optimized with state-averaged orbitals. The geometry of the squaraine fragment is found to be very similar to that of the D_{2h} S_1 transition state found for the isolated model squaraine chromophore (Figure 6). An adjacent sloped conical intersection was optimized between S_0 and S_1 (see Figure 10 and the inset in Figure 2 region B). The excited-state complex lies 69 kcal mol^{-1} below the FC region. This energy difference provides the driving force for the formation of the excited-state complex while the sloped conical intersection provides the mechanism for the charge-injection process.

The two degenerate states of the squaraine−TiO_2 conical intersection near the excited-state complex can be characterized

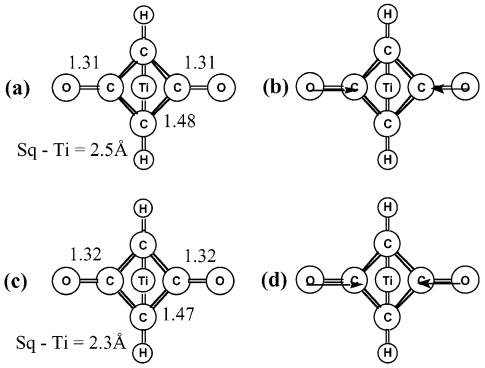

Figure 11. (a) S_0 IRD geometry. (b) Gradient at S_0 IRD. This path leads along a valley to the $Sq^{\cdot+}/TiO_2^{\cdot-}$ minimum. (c) S_1 IRD geometry. (d) Gradient at S_1 IRD. This path leads to the excited complex minimum. Both IRDs and associated gradients are similar which is indicative of a sloped topology. (Bond lengths in angstroms.)

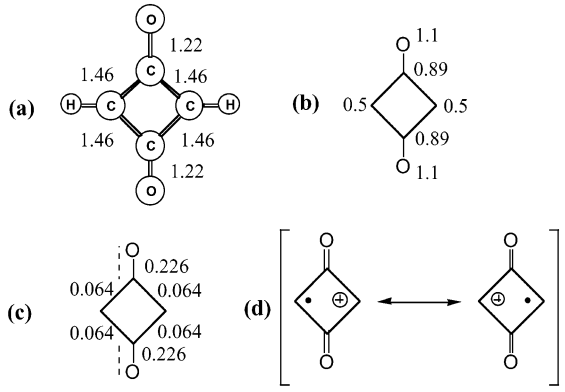

Figure 12. (a) S_0 minimum geometry of model squaraine chromophore radical cation ($Sq^{\cdot+}$). (b) One-electron p_π atomic orbital densities calculated from localized orbitals. (c) Spin-exchange density matrix elements (P_{ij}). (d) Representative valence bond structure of $Sq^{\cdot+}$ at S_0 minimum. The positive charge is delocalized over the two C−H carbons and the CO bonds are coupled as double bonds. (Bond lengths in angstroms.)

as follows. In one state, the six π-electrons are localized in orbitals on the squaraine fragment and there is almost negligible electron density on the titanium. In the other state, five electrons are localized on the squaraine and there is significant electronic density (ca 1.2 electrons) delocalized between the squaraine and the TiO_2. The primary orbitals involved are given as Supporting Information.

We now discuss the topology of the conical intersection shown in Figure 10 and the reaction paths emanating from it. IRD searches on both the S_0 and S_1 surfaces (see Computational Details) were performed using the gradient difference (GD) (Figure 10b) and derivative coupling (DC) (Figure 10c) directions as initial search directions. On S_0 only a single IRD could be found and the initial IRC vectors (as characterized by the gradient) are shown in Figure 11b,d. It can be seen that the gradients lie almost parallel to the GD vector and are dominated by the CO stretch.

The charge transfer species lies along this coordinate. Computations on the radical cation of the model squaraine chromophore were performed using a CASSCF wave function with five π electrons distributed in six p_π molecular orbitals. The symmetry of the ground state of the radical cation is $^2B_{3u}$ and the S_0 minimum geometry has D_{2h} symmetry (Figure 12(a)). The P_{ij} values calculated at this geometry are given in Figure 12c, and the value of +0.226 for the CO coupling shows that the CO bonds are coupled as double bonds. The one electron

density (Figure 12b) shows that there is a density of exactly $0.5e^-$ at each of the C−H carbons. This is consistent with the electronic structure being a resonance of the structures in Figure 12d. The positive charge has become delocalized on the two central C−H carbons.

We now resume our discussion of the IRD in the region of the squaraine−TiO_2 conical intersection. The S_0 state corresponds to the charge-transfer state (i.e., $Sq^{\cdot+}/TiO_2^{\cdot-}$). The fact that only one IRD is found from two orthogonal search directions indicates that the conical intersection has a sloped topology. The gradient of the IRD point on S_0 is seen to involve essentially CO bond contraction. This is consistent with the squaraine relaxing to the ground-state minimum of the radical cation of the model chromophore (Figure 12), where the CO bonds are recoupled. A full IRC was run from this IRD and terminated at a geometry where the squaraine radical cation was similar to that shown in Figure 12. The IRC describes the valley on the S_0 surface which leads to the charge-transfer products (Figure 2). Details of the IRC are given as Supporting Information.

The S_1 state corresponds to the neutral (locally excited) species (Sq^*/TiO_2). The same IRD search directions were used on this surface (i.e., the GD and DC vectors) and again only one IRD was found (Figure 11c). This IRD also has a gradient which lies parallel to the GD vector (Figure 11c). The IRDs found on S_0 and S_1 are very similar (almost parallel) which is also compelling evidence that the conical intersection has a sloped topology. An IRC started from the S_1 IRD leads to the S_1 excited complex minimum. The gradient at the S_1 IRD involves contraction of the CO bonds and a slight increase in the squaraine/TiO_2 separation.

Discussion

Charge Injection vs Unreactive Decay. We have completed our documentation of the reaction path for the charge transfer in our model squaraine−TiO_2 system, and now discuss the mechanistic implications indicated schematically in Figure 2. The reaction path begins with the two species (Sq and TiO_2) on the ground state separated by at least the sum of the carbon and titanium van der Waals radii. The system is excited at 532 nm to give a locally excited $\pi-\pi^*$ state of the squaraine. Along the Sq−Ti intermolecular separation coordinate the S_1 potential is strongly attractive (the excited-state complex minimum is 69 kcal mol^{-1} lower in energy than the FC point). The titanium is attracted to the electron rich ring of the squaraine. In the squaraine moiety, the system will also relax along the CO bond length coordinate toward a geometry similar to the isolated S_1 D_{2h} minimum (Figure 6). Thus after excitation, the system will relax along both of these coordinates in order to reach the excited complex minimum (Figure 9) and will then decay to the ground state via the charge-transfer conical intersection (Figure 10). However, there is also the competitive nonreactive photophysical pathway. The locally excited chromophore can decay to the ground state in region A, via a recoupling of the π-electron system discussed for the isolated squaraine chromophore. The decay to the ground state can occur at any point along a seam of intersection between region A and region B.

The energy gap between the S_1 minimum and the sloped conical intersection (see Table 1) is slightly higher than one would expect for an electron-transfer reaction. One would expect an almost barrierless process whereas our model has a calculated energy gap of around 9 kcal mol^{-1}. However, we have investigated a simple model of a complex system and would not expect this model to give perfect energetics. Thus, our model provides qualitative mechanistic information regarding the electron-transfer process. It is possible that the energy gap would be lowered in an extended model or by taking account of dynamical electron correlation energy (e.g. calculating a second-order perturbation theory correction to the energies).

Gas-Phase Results vs Solid State. Our calculations on the gas-phase charge transfer for the squaraine−TiO_2 model do not account explicitly for dynamic effects or for the fact that the charge injection in the solid-state involves a TiO_2 surface with a conduction band rather than an acceptor orbital. Thus, we have calculated the minimum energy paths for the charge-injection step, but clearly real trajectories for vibrationally hot states will not follow this path. Vibrational modes can induce the decay at any point along the seam shown in Figure 2 (see the discussion above). Moreover, our results suggest that the C−O symmetric stretching mode will play a predominant role in the dynamics. The exciplex formation and the radiationless decay coordinate involve the Sq−Ti distance and the C−O stretching coordinate. This bond is stretched from 1.19 Å in the isolated ground-state dye (Figure 3) to 1.28 Å in the exciplex (Figure 9) and 1.34 Å at the conical intersection (Figure 10). Thus, in the classical dynamics picture, the molecule will accumulate enough energy in the C−O stretching mode during the decay from the FC region (exciplex formation) to reach the seam by further bond stretching. In other words, after electronic excitation, the C−O stretch of the molecule is vibrationally excited, and this increases the probability of electron transfer (ET) because the neutral and charge transfer (CT) states are coupled along that mode (see Figure 11). Moreover, the charge transfer to the conduction band of the solid can be thought of as the superposition of a series of crossings between the locally excited state of the dye and a series of close-lying charge-transfer states (see for example simulations for photoinduced heterogeneous electron transfer using a finite electronic-vibrational quasicontinuum for the simulation of the conduction band[34]). The charge-injection efficiency in the real, solid-state system will then be increased with respect to our gas-phase model because there is a manifold of crossings available for the charge injection.

Marcus-Type Characterization of the Charge Injection. In the Marcus description of electron transfer, the inverted region occurs when the two minima that correspond to the donor-acceptor pair before and after the electron transfer lie on the same side of the crossing between the two diabatic states.[35] One of the minima lies on the ground state, and the other on the excited-state potential energy surface. For our model, this applies to the third step of the mechanism outlined in eq 1 i.e., the electron transfer that leads from the excited-state complex to the charge-transfer pair (see the inset B on the right side of Figure 2). Thus, the last step of the photoinjection mechanism described here is a case of electron transfer in the inverted region which is equivalent to nonradiative decay through a sloped conical intersection, a real crossing of adiabatic states. However, it should be noted that strictly it is only valid to talk about an inverted Marcus region in the gas phase or in solution. In the solid state, the distinction between normal and inverted Marcus regions is blurred because the charge-transfer state is virtually a superposition of states (see the quasi-continuum calculations of ref 34).

The correspondence must be a general property, since previous calculations for ground-state electron transfer have proved that in the full space of nuclear degrees of freedom, the Marcus crossing region is centered on a conical intersection.[20] However, in the limiting case of strong coupling between the states, the crossing will be avoided and the conical intersection

TABLE 2: Energetics of Squaraine−TiO_2 Complex

	energy (au)	ΔE (relative to S_1 minumum, kcal mol^{-1})
S_1 LE complex minimum (Figure 9)	−1300.2267	0.0
$S_{0/1}$ charge-transfer CI (Figure 10a)	−1300.2110	9.8
S_1 FC (inf sep) (Sq S_1 FC + RHF TiO_2)	−1300.1160	69.4

TABLE 3: Classification of Electron-Transfer Reactions According to Degree of Coupling and Type of Marcus Surface (Tunneling Not Considered)

	weak coupling	strong coupling
normal region	thermal, nonadiabatic	thermal, adiabatic
inverted region	activated (nonradiative), nonadiabatic	radiative, nonadiabatic

will be too high in energy to be accessed thermally. In that case, the electron transfer in the inverted region will occur as a radiative process (not considering tunneling). It appears that the main difference between electron transfer in the normal and inverted Marcus regions, concerns the coupling between the states (see Table 3). In the normal region, strong coupling leads from nonadiabatic to adiabatic thermal electron transfer and an *increase* in the reaction rate. However, in the inverted region, electron transfer will always be nonadiabatic and strong coupling will change the reaction from activated (nonradiative) to radiative. Therefore, strong coupling will lead to a *decrease* in the rate constant, because the nonradiative path through the crossing is switched off. On the other hand, very weak coupling (i.e. virtually zero) will also lower the reaction rate. There will be an intermediate region of weak, nonzero coupling where the rate is maximal.

In fact, radiative electron transfer has been measured experimentally in the recovery of the neutral ground state from an excited-state charge-transfer species, in some organic donor−bridge-acceptor systems.[36] This is a case of strong coupling in the inverted region, where the reaction times lie in the nanosecond regime, which is typical for radiative processes. The nonradiative electron transfer considered here, which occurs in an inverted Marcus region with weak coupling, is significantly faster and takes place in picoseconds.

The present photoinduced electron injection can be classified as a three-state process, analogous to bridge mediated, ground-state electron transfer.[20,37−39] The three states are represented in a Marcus−Hush type diagram in Figure 13. Three-state diagrams for photoinduced electron transfer have been proposed before,[40] and usually consist of one ground-state (usually U_{neut}) and two excited states (U_{CT} and U_{LE}). However, the present situation has two ground-state diabats and one for the excited state, because the product ion pair is a ground-state species. The dashed parabolas are the diabatic states for the neutral pair (U_{neut}), the ion pair (U_{CT}), and the pair with local excitation on the squaraine (U_{LE}). For simplicity, U_{neut} and U_{CT} are taken to be symmetric (the curves would have to be displaced to reproduce the situation studied here more accurately). The full lines represent the adiabatic states, i.e., the result of our ab initio calculations. In a Marcus−Hush treatment, these states are obtained by coupling the diabatic surfaces. The Marcus−Hush diagram of Figure 13 thus reproduces a cut of our schematic potential energy surface along the Sq−Ti coordinate. The photoinduced electron transfer analyzed here can be rationalized together with bridge-mediated, ground-state electron transfer, using a common model where U_{LE} is replaced by a bridge state (charge localized on the bridge). Conceptually, the two states involved in the charge transfer are connected by an "auxiliary" state that mediates the process, although in two completely

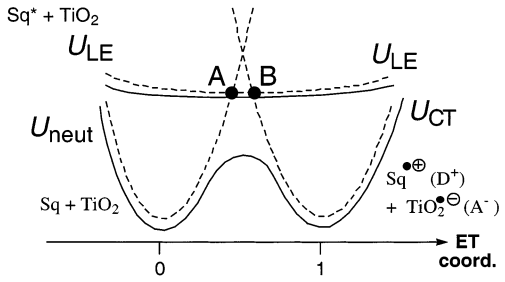

Figure 13. Marcus−Hush diagram for the charge-transfer process. Dashed lines are diabatic potentials and solid lines are the adiabatic potentials.

different ways. In the ground-state electron transfer the bridge state is coupled to the two other states in the central part of the diagram (halfway through the reaction coordinate), and lowers the ground-state activation energy. Therefore, in this case the key region for the electron transfer is the transition state region on the lower adiabatic state (full line). In the photoinduced case studied here, however, the electron transfer is facilitated by populating the "auxiliary" state U_{LE} photochemically. The key region for the photoinduced electron transfer is the seam for the radiationless decay. In our Marcus−Hush type diagram, the two regions of the seam that lead to unreactive decay and electron transfer are represented by black dots at the crossings between U_{LE} and U_{neut}, and $U_{LE\ and}$ U_{CT}, respectively. These points correspond to the regions A and B shown in Figure 2. In the full space of vibrational modes, these two points are connected and form a seam of intersection.

Conclusions

The mechanistic features of the photoinduced charge-injection process from a squaraine dye to a large band gap semiconductor have been modeled with a simple TiO_2 − squaraine complex. The main driving forces for the reaction are the electronic character of the $\pi-\pi^*$ excitation of the chromophore and the stability of the final product (charge-transfer $Sq^{\cdot+}$ and $TiO_2^{\cdot-}$ pair). The singlet $\pi-\pi^*$ excitation increases the electron density in the squaraine ring by charge transfer from the oxygen atoms, and this favors the formation of an excited-state complex between the excited squaraine molecule and TiO_2. The final radical ion pair ($Sq^{\cdot+}$ and $TiO_2^{\cdot-}$) lies on the ground electronic state of the system. Therefore, the charge transfer between the excited chromophore and the TiO_2 is an ultrafast chemical process coupled to radiationless decay. The decay occurs through a conical intersection, and, because of the sloped topology, the only product is the radical ion pair. For the last step of the process (the electron transfer between the two molecules), the sloped conical intersection topology corresponds to an inverted Marcus region.

An alternative radiationless decay pathway exists and involves a recoupling of the π-electron system on the locally excited squaraine. If the squaraine and the TiO_2 are very far apart this alternative decay pathway will compete with the charge transfer. When the squaraine is "anchored" to the semiconductor surface the excited complex will form more often and the electron-transfer rate constants will be higher.

Our model gives a mechanistic explanation of the interfacial intermolecular charge transfer between a squaraine dye and TiO_2 which is consistent with experimental studies on the charge-injection dynamics. We also speculate that it should be possible to increase the electron-transfer rate constant by first "anchoring" the squaraine dye to the semiconductor surface using suitable

substituent groups, then coherently exciting the symmetric CO stretching mode of the squaraine.

Acknowledgment. All computations were carried out on an IBM-SP2 funded jointly by IBM-UK and HEFCE (UK). Financial support for this project was provided by EPSRC (UK) under grant number 98312744.

Supporting Information Available: Cartesian coordinates of all optimized geometries, orbital plot of primary orbitals involved in charge-transfer process, Cartesian coordinates of all IRD geometries (and gradients at IRDs), and IRC data. This material is available free of charge via the Internet at http://pubs.acs.org.

References and Notes

(1) Tam, A. C. *Appl. Phys. Lett*. **1980**, *37*, 978.
(2) Law, K.-Y. *J. Phys. Chem*. **1988**, *92*, 4226.
(3) Emmelius, M.; Pawlowski, G.; Vollmann, H. W. *Angew. Chem., Int. Ed. Engl*. **1989**, *28*, 1445.
(4) Law, K.-Y. *Chem. Rev*. **1993**, *93*, 449−486.
(5) Liu, D.; Kamat, P. V.; Thomas, K. G.; Thomas, K. J.; Das, S.; George, M. V. *J. Chem. Phys*. **1997**, *106*, 6404−6411.
(6) Kamat, P. V.; Das, S.; Thomas, K. G.; George, M. V. *Chem. Phys. Lett*. **1991**, *178*, 75−79.
(7) Das, S.; Thomas, K. G.; George, M. V. In *Molecular and Supramolecular Photochemistry, Vol. 1: Organic Photochemistry*; Ramamurthy, V., Schanze, K. S., Eds.; 1997; Chapter 11.
(8) Wang, C.; Liu, C.; Wang, W.; Shen, T. *J. Photochem. Photobiol., A* **1997**, *109*, 159−164.
(9) Sauve, G.; Kamat, P. V.; Thomas, K. G.; Thomas, K. J.; Das, S.; George, M. V. *J. Phys. Chem*. **1996**, *100*, 2117−2124.
(10) Robb, M. A.; Garavelli, M.; Olivucci, M.; Bernardi, F. *Rev. Comput. Chem*. **2000**, *15*, 87−146.
(11) Sanchez-Galvez, A.; Hunt, P.; Robb, M. A.; Olivucci, M.; Vreven, T.; Schlegel, H. B. *J. Am. Chem. Soc*. **2000**, *122*, 2911−2924.
(12) Garavelli, M.; Bernardi, F.; Olivucci, M.; Vreven, T.; Klein, S.; Celani, P.; Robb, M. A. *Faraday Discuss*. **1998**, *110*, 51−70.
(13) Bernardi, F.; Olivucci, M.; Robb, M. A. *Chem. Soc. Rev*. **1996**, *25*(5), 321.
(14) Rehm, J. M.; McLendon, G. L.; Nagasawa, Y.; Yoshihara, K.; Moser, J.; Grätzel, M. *J. Phys. Chem*, **1996**, *100*, 9577.
(15) Burfeindt, B.; Hannappel, T.; Storck, W.; Willig, F. *J. Phys. Chem*. **1996**, *100*, 16463.
(16) Atchity, G. J.; Xantheas, S. S.; Ruedenberg, K. *J. Chem. Phys*. **1991**, *95*, 1862−1876.
(17) Bearpark, M. J.; Robb, M. A.; Schlegel, H. B. *Chem. Phys. Lett*. **1994**, *223*, 269−274.
(18) Stier, W.; Prezhdo, O. V. *J. Phys. Chem. B* **2002**, *106*, 8047−8054.
(19) Barbara, P. F.; Meyer, T. J.; Ratner, M. A. *J. Phys. Chem*. **1996**, *100*, 13148−13168.
(20) Fernández, E.; Blancafort, L.; Olivucci, M.; Robb, M. A. *J. Am. Chem. Soc*. **2000**, *122*, 7528−7533.
(21) Becke, A. D. *J. Chem. Phys*. **1993**, *98*, 1293.
(22) Stratmann, R. E.; Scuseria, G. E.; Frisch, M. J. *J. Chem. Phys*. **1998**, *109*, 8218−8224.
(23) Bernardi, F.; Celani, P.; Olivucci, M.; Robb, M. A.; Suzzi-Valli, G. *J. Am. Cham. Soc*. **1995**, *117*, 10531−10536.
(24) Boys, S. F. *Rev. Mod. Phys*. **1960**, *32*, 296.
(25) Celani, P.; Robb, M. A.; Garavelli, M.; Bernardi, F.; Olivucci, M. *Chem. Phys. Lett*. **1995**, *243*, 1−8.
(26) Frisch, M. J.; Trucks, G. W.; Schlegel, H. B.; Scuseria, G. E.; Robb, M. A.; Cheeseman, J. R.; Zakrzewski, V. G.; Montgomery, J. A., Jr.; Stratmann, R. E.; Burant, J. C.; Dapprich, S.; Millam, J. M.; Daniels, A. D.; Kudin, K. N.; Strain, M. C.; Farkas, O.; Tomasi, J.; Barone, V.; Cossi, M.; Cammi, R.; Mennucci, B.; Pomelli, C.; Adamo, C.; Clifford, S.; Ochterski, J.; Petersson, G. A.; Ayala, P. Y.; Cui, Q.; Morokuma, K.; Malick, D. K.; Rabuck, A. D.; Raghavachari, K.; Foresman, J. B.; Cioslowski, J.; Ortiz, J. V.; Stefanov, B. B.; Liu, G.; Liashenko, A.; Piskorz, P.; Komaromi, I.; Gomperts, R.; Martin, R. L.; Fox, D. J.; Keith, T.; Al-Laham, M. A.; Peng, C. Y.; Nanayakkara, A.; Gonzalez, C.; Challacombe, M.; Gill, P. M. W.; Johnson, B. G.; Chen, W.; Wong, M. W.; Andres, J. L.; Head-Gordon, M.; Replogle, E. S.; Pople, J. A. *Gaussian 98*, Revision C.1; Gaussian, Inc., Pittsburgh, PA, 1998.
(27) Kamat, P. V.; Das, S.; Thomas, K. G.; George, M. V. *J. Phys. Chem*. **1992**, *96*, 195−199.
(28) Zhao, W.; Chen, J.; Zhang, B.; Cao, Y. *Dyes Pigm*. **1998**, *39*, 281−290.
(29) Law, K.-Y. In *Molecular and Supramolecular Photochemistry, Vol. 1: Organic Photochemistry;* Ramamurthy, V., Schanze, K. S., Eds.; 1997; Chapter 12.
(30) Bigelow, R. W.; Freund, H.-J. *Chem. Phys*, **1986**, *107*, 159−174.
(31) Gude, C.; Rettig, W. *J. Phys. Chem. A* **2000**, *104*, 8050−8057.
(32) Glassford, K. M.; Chelikowsky, J. R. *Phys. Rev. B* **1992**, *46*, 1284−1298.
(33) Wu, H.; Wang, L.-S. *J. Chem. Phys*. **1997**, *107*, 8221−8228.
(34) Ramakrishna, S.; Willig, F.; May, V. *J. Chem. Phys*. **2001**, *115*, 2743−2756.
(35) Sutin, N. *Prog. Inorg. Chem*. **1983**, *30*, 441−498.
(36) Smit, K. J.; Warman, J.; De Haas, M. P.; Paddon-Row, M. N.; Oliver, A. M. *Chem. Phys. Lett*. **1988**, *152*, 177.
(37) Cannon, R. D. In *Electron-Transfer Reactions*; Butterworth: London, 1980; 223−237.
(38) Newton, M. D. *Chem. Rev*. **1991**, *91*, 767−792.
(39) Nelsen, S. F.; Ismagilov, R. F.; Powell, D. R. *J. Am. Chem. Soc*. **1998**, *120*, 1924−1925.
(40) Bixon, M.; Jortner, J.; Verhoeven, J. W. *J. Am. Chem. Soc*. **1994**, *116*, 7349−7355.